Electronic Supplementary Information for:

Modulation of Pore Shape and Adsorption Selectivity by Ligand Functionalization in a Series of "rob"-like Flexible Metal-Organic Frameworks

Javier Cepeda,[a] Manuel Pérez-Mendoza,[b] Antonio J. Calahorro,[b] Nicola Casati,[c] José Manuel Seco,[a] Marta Aragones-Anglada,[d] Peyman Z. Moghadam,[d] David Fairen-Jimenez[d,] and Antonio Rodríguez-Diéguez[b,*]*

[a]Departamento de Química Aplicada, Facultad de Química, Universidad del País Vasco/Euskal Herriko Unibertsitatea (UPV/EHU), 20018 San Sebastián, Spain.

[b]Departamento de Química Inorgánica, Universidad de Granada, 18071 Granada, Spain.

[c]Paul Scherrer Institute, 5232 Villigen, Switzerland.

[d]Adsorption & Advanced Materials Laboratory (AAML), Department of Chemical Engineering & Biotechnology, University of Cambridge, United Kingdom. E-mail: df334@cam.ac.uk.

Contents: **Page no.**

S1. Materials and Measurements.

All chemicals were of reagent grade and were used as commercially obtained. Thermal analysis (TG/DTA) was performed on a TA Instruments SDT 2960 thermal analyser from room temperature up to 800 ºC in a synthetic air atmosphere (79% N_2 / 21% O_2) with a heating rate of 5 ºC/min. Elemental analyses (C, H, and N) were performed on a Fisons Instruments EA-1008 analyser. Metal content was determined by inductively coupled plasma (ICP-AES) analysis with a Horiba Yobin Yvon Activa spectrometer. The IR spectrum (KBr pellets) was recorded on a ThermoNicolet IR 200 spectrometer in the 4000−400 cm^{-1} spectral region.

X-ray powder diffraction (XRPD) pattern was collected on a Phillips X'PERT powder diffractometer with Cu-Kα radiation (λ = 1.54060 Å) over the 5 < 2θ < 50º range with a step size of 0.026º and an acquisition time of 2.5 s per step at 25 ºC. Indexation of the diffraction profiles were made by means of the FULLPROF program (pattern-matching analysis) on the basis of the space group and the cell parameters found for compound **1** with single crystal X-ray diffraction.

S2. X-ray Data Collection and Structure Determination.

Table S1. Selected bond lengths for **GR-MOF-2**.[a]

Cu1–O1B	1.974(2)	Cu1–O9B(iii)	1.970(2)
Cu1–O2B(i)	1.974(2)	Cu1–N1A	2.179(2)
Cu1–O8B(ii)	1.973(2)	Cu1···Cu1(i)	2.632(6)

[a] Symmetries: (i) –x + 1/2, –y + 1/2, –z; (ii) –x + 1/2, y + 1/2, –z + 1/2; (iii) x, –y, –z + 1/2.

Table S2. Selected bond lengths for **GR-MOF-3**.[a]

Cu1–O1B	1.967(4)	Cu1–O9B(iii)	1.974(4)
Cu1–O2B(i)	1.969(4)	Cu1–N1A	2.162(4)
Cu1–O8B(ii)	1.967(4)	Cu1···Cu1(i)	2.613(2)

[a] Symmetries: (i) –x + 1/2, –y – 1/2, –z; (ii) –x + 1/2, y + 1/2, –z + 3/2; (iii) x, –y – 1, –z – 1/2.

Table S3. Selected bond lengths for **GR-MOF-4**.[a]

Cu1–O1B	1.956(3)	Cu1–O9B(iii)	1.965(3)
Cu1–O2B(i)	1.970(3)	Cu1–N1A	2.168(3)
Cu1–O8B(ii)	1.966(3)	Cu1···Cu1(i)	2.604(1)

[a] Symmetries: (i) –x + 3/2, –y + 1/2, –z; (ii) –x + 3/2, y + 1/2, –z + 1/2; (iii) x, –y, –z + 1/2.

Table S4. Selected bond lengths for **GR-MOF-5**.[a]

Cu1–O1B	1.973(2)	Cu1–O9B(iii)	1.976(2)
Cu1–O2B(i)	1.971(2)	Cu1–N1A	2.179(2)
Cu1–O8B(ii)	1.975(2)	Cu1···Cu1(i)	2.625(6)

[a] Symmetries: (i) –x + 3/2, –y + 1/2, –z + 1; (ii) –x + 1/2, y + 3/2, –z + 1/2; (iii) x + 1, –y – 1, –z + 3/2.

S3. Continuous shape measurements (CShMs).

Continuous shape measurements were performed by means of SHAPE program,[1] by which the shape of the polyhedron is compared to most common polyhedra containing five donor atoms.

Table S5. Continuous shape measurements for the CuNO4 coordination environment of **GR-MOF** compounds.

PP-5	D5h	Pentagon
vOC-5	C4v	Vacant octahedron
TBPY-5	D3h	Trigonal bipyramid
SPY-5	C4v	Spherical squrare pyramid
JTBPY-5	D3h	Johnson trigonal bipyramid

GR-MOF	PP-5	vOC-5	TBPY-5	SPY-5	JTBPY-5
2	30.59	0.80	5.97	0.54	8.42
3	30.66	0.76	5.95	0.56	8.36
4	30.61	0.70	5.91	0.52	8.33
5	30.33	0.77	6.01	0.57	8.43

[1] M. Llunell, D. Casanova, J. Cirera, J. M. Bofill, P. Alemany, S. Alvarez, M Pinsky and D. Avnir, SHAPE v1.7, University of Barcelona, Barcelona, 2010.

S4. Thermogravimetric Analysis.

All compounds show a similar thermal behaviour consisting in a first endothermic loss corresponding to the lattice water molecules (4 H_2O per formula unit). The loss of these molecules is progressive in this experiment and completes below 200 ºC in all cases. Then, GRMOFs are slowly decomposed to yield CuO above 400 ºC.

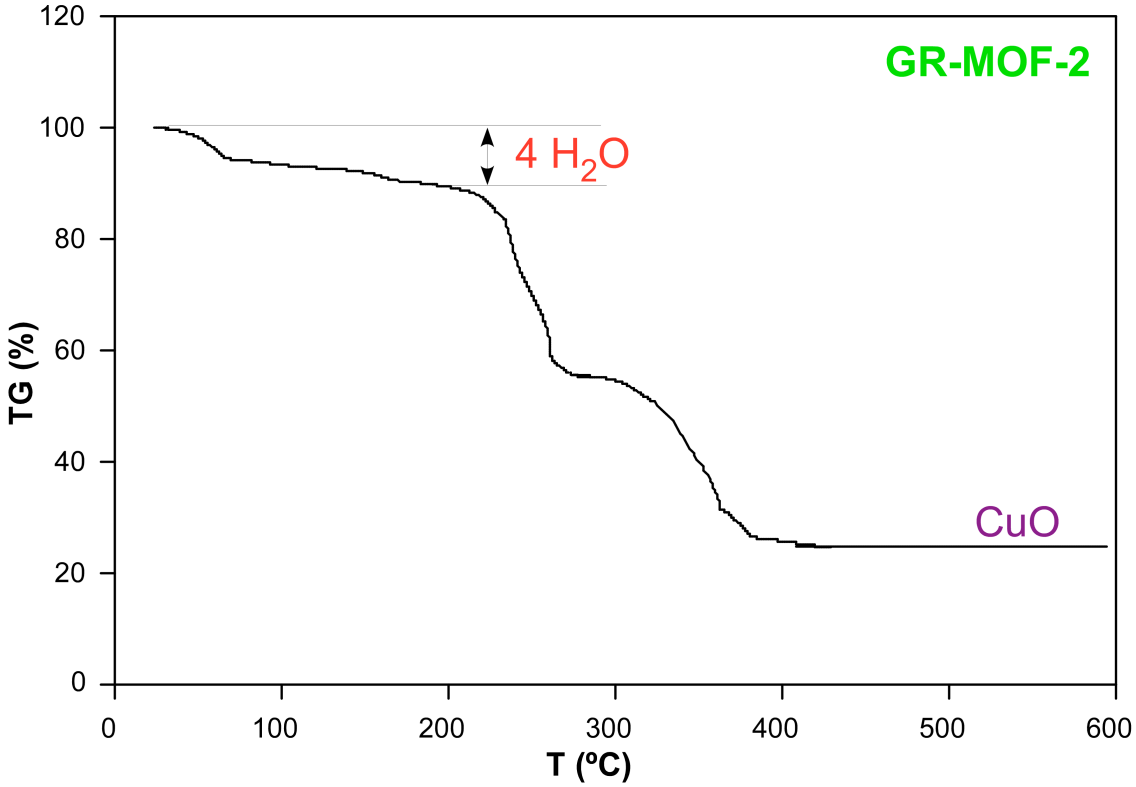

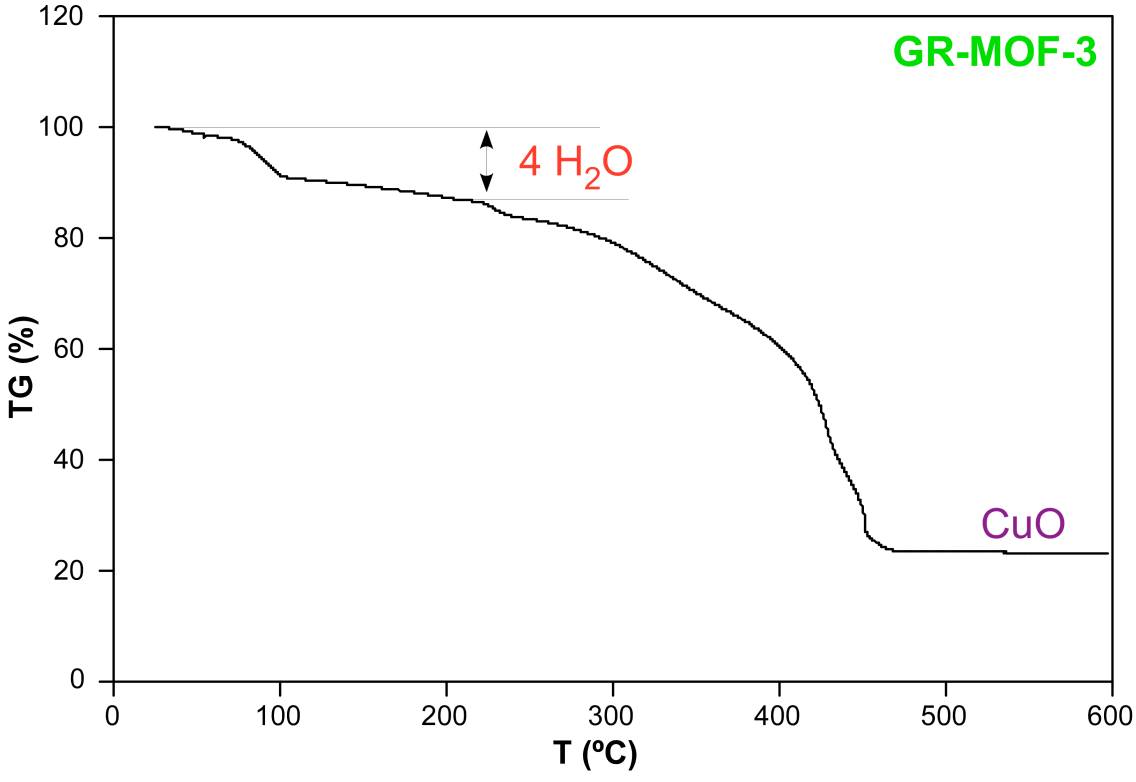

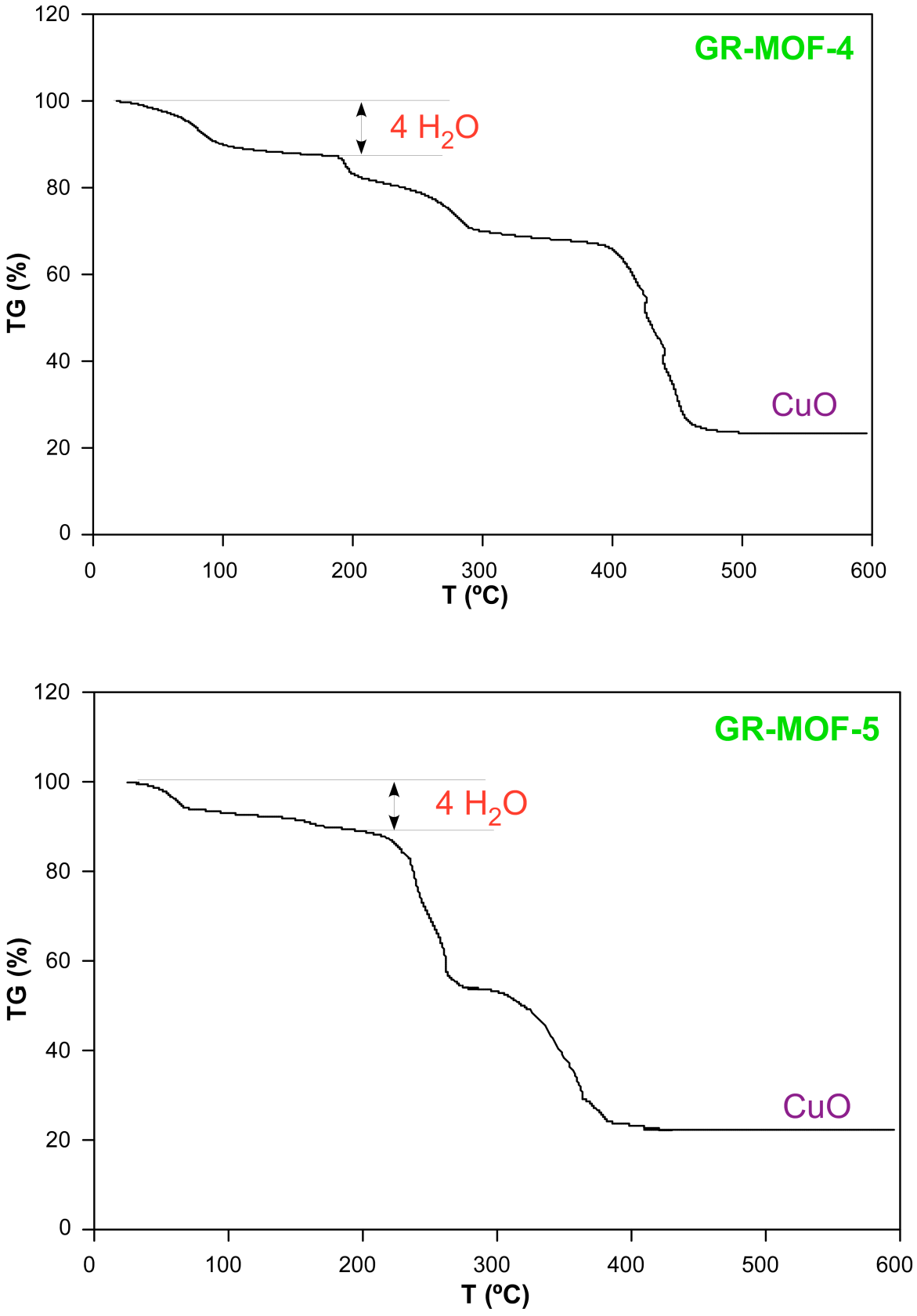

Figure S1. Thermogravimetric curves for **GR-MOFs**.

S5. Powder X-ray Diffraction Analysis.

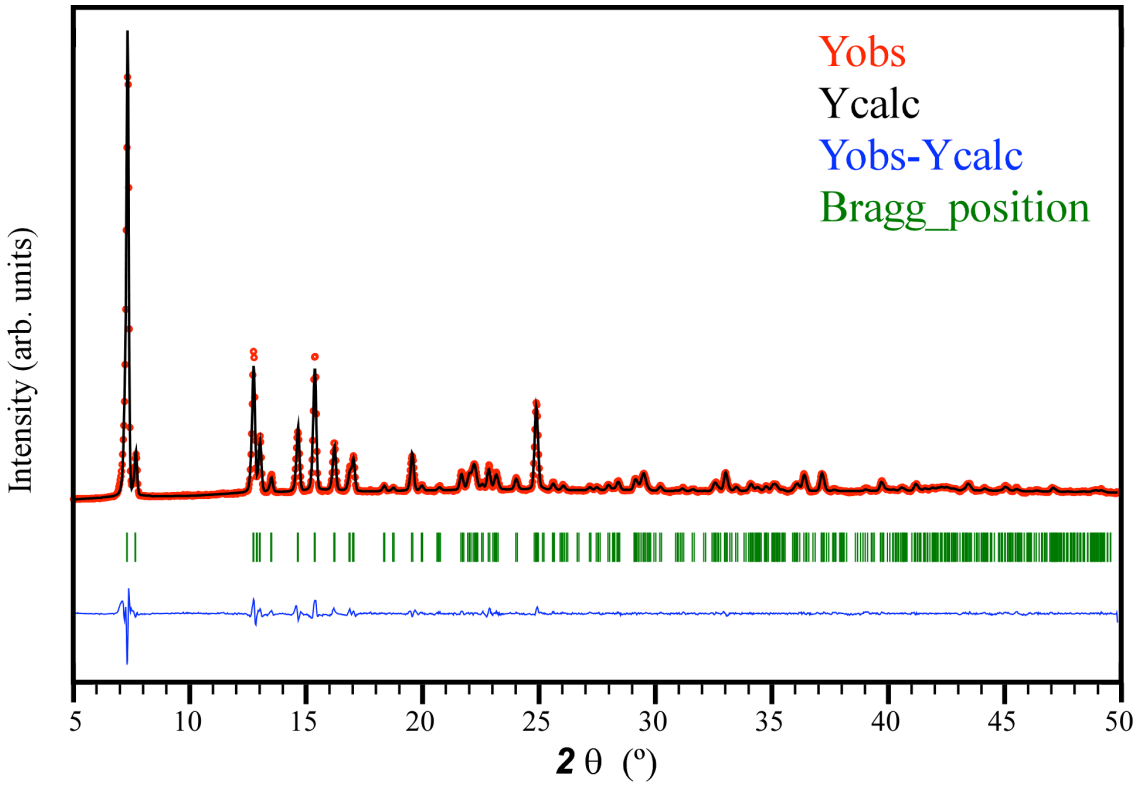

Figure S2. Pattern-matching analysis (Le Bail fitting) of polycrystalline sample of **GR-MOF-2**.

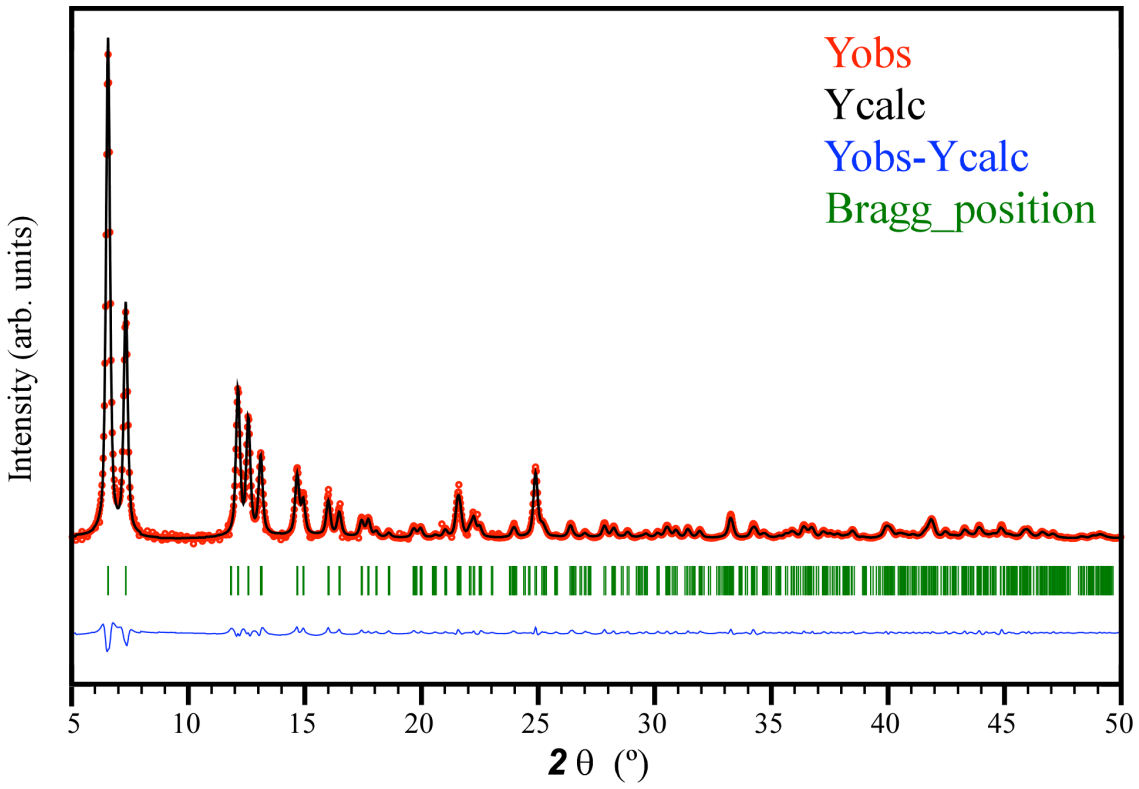

Figure S3. Pattern-matching analysis (Le Bail fitting) of polycrystalline sample of **GR-MOF-3**.

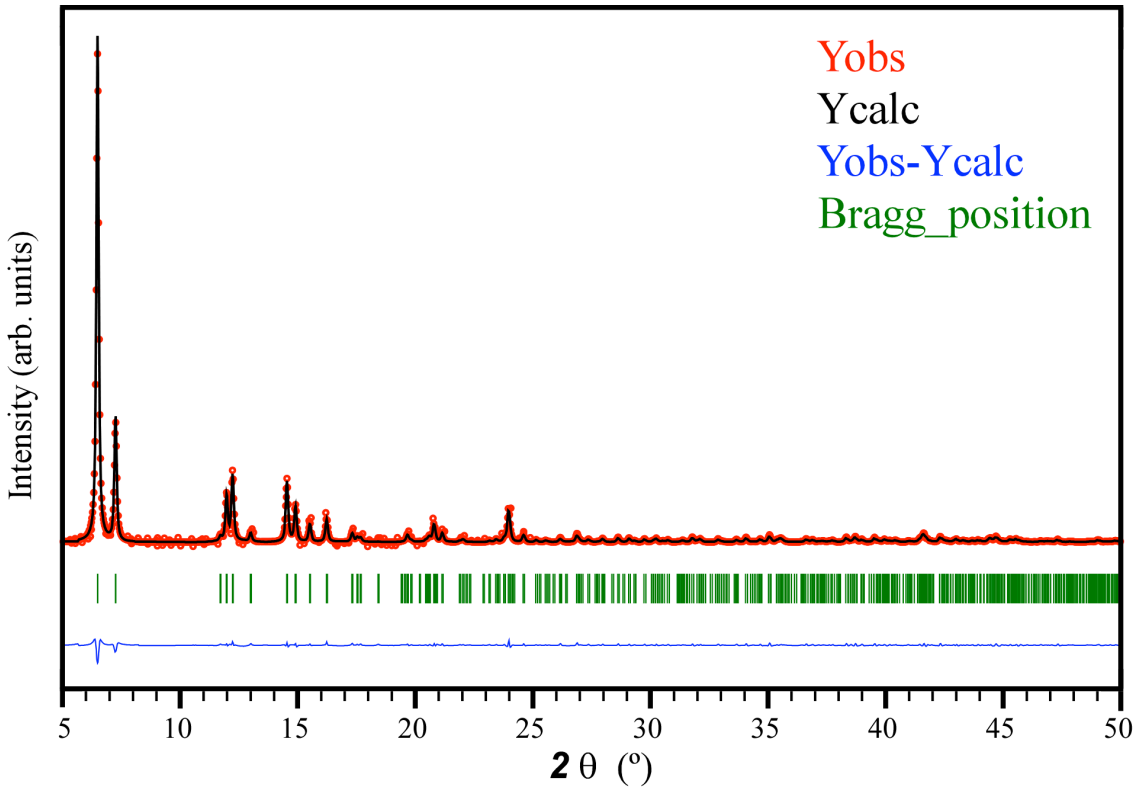

Figure S4. Pattern-matching analysis (Le Bail fitting) of polycrystalline sample of **GR-MOF-4**.

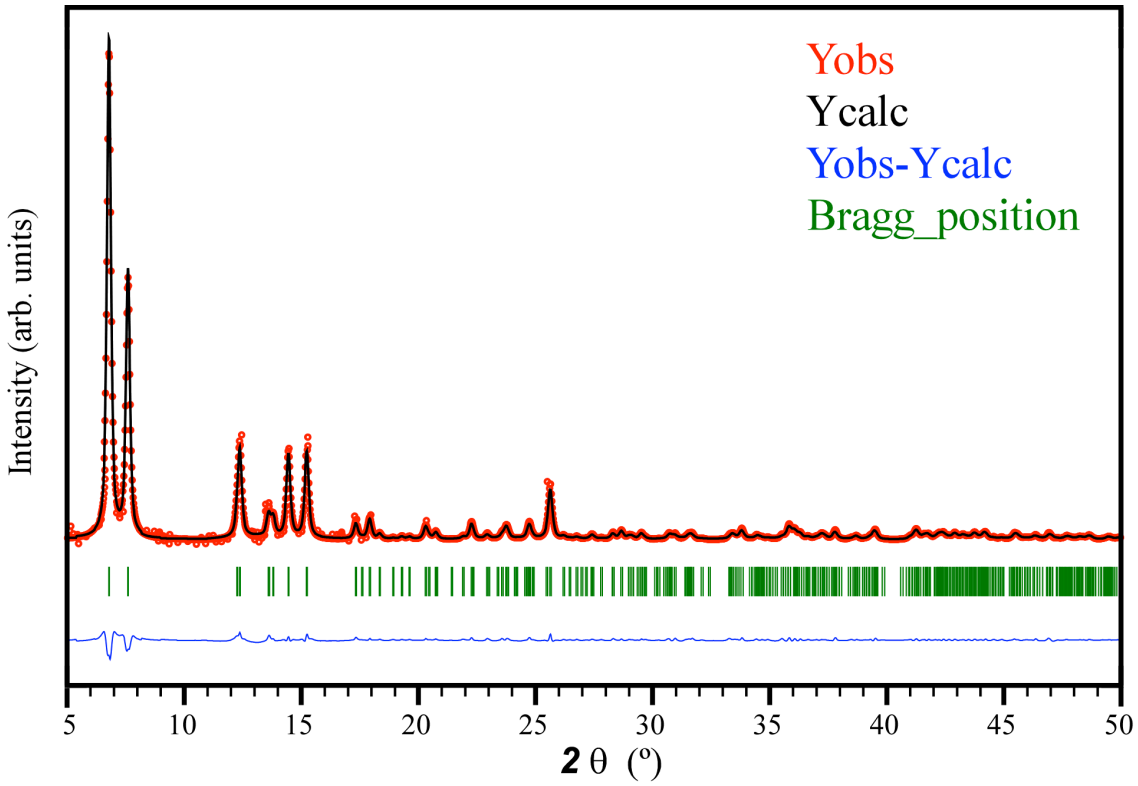

Figure S5. Pattern-matching analysis (Le Bail fitting) of polycrystalline sample of **GR-MOF-5**.

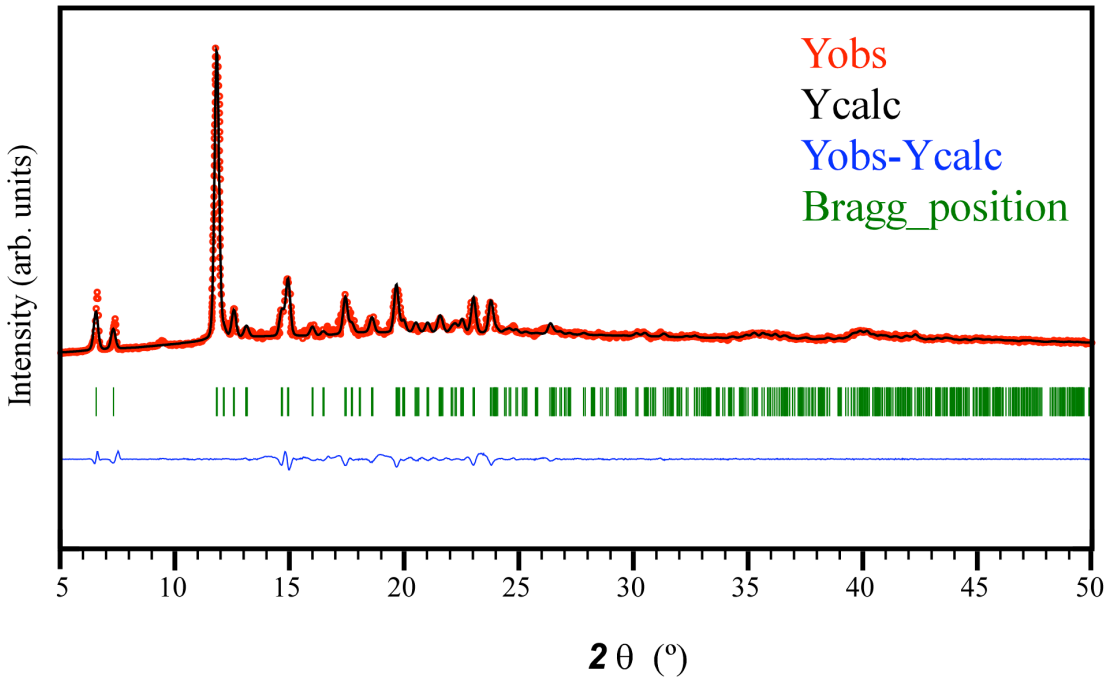

Figure S6. Pattern-matching analysis (Le Bail fitting) of activated polycrystalline sample of **GR-MOF-3**.

S6. Additional figures.

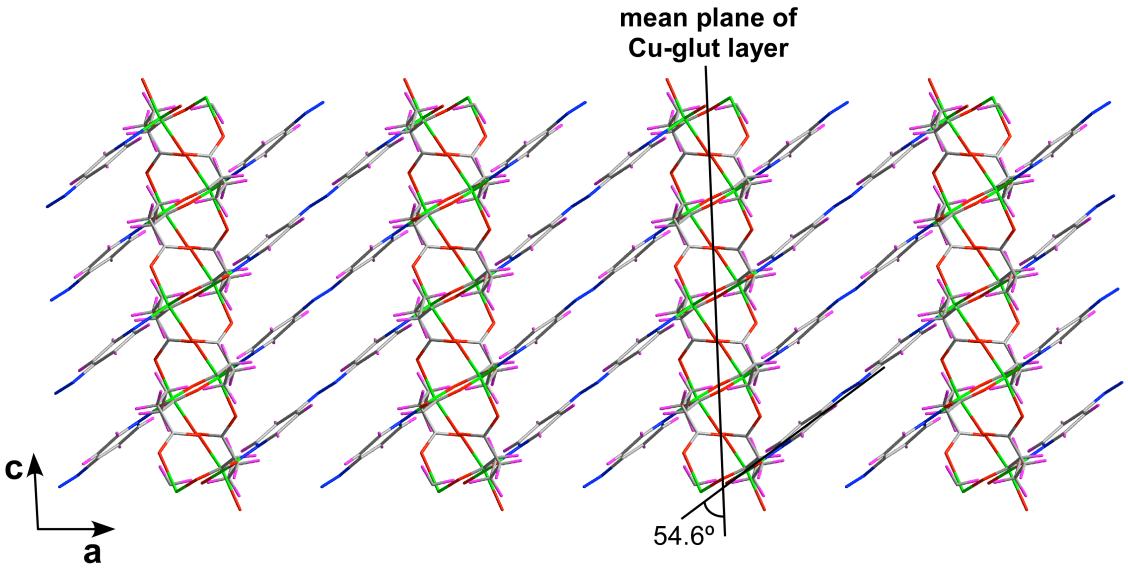

Figure S7. Crystal packing of **GR-MOF-2** in which lattice water molecules have been omitted.

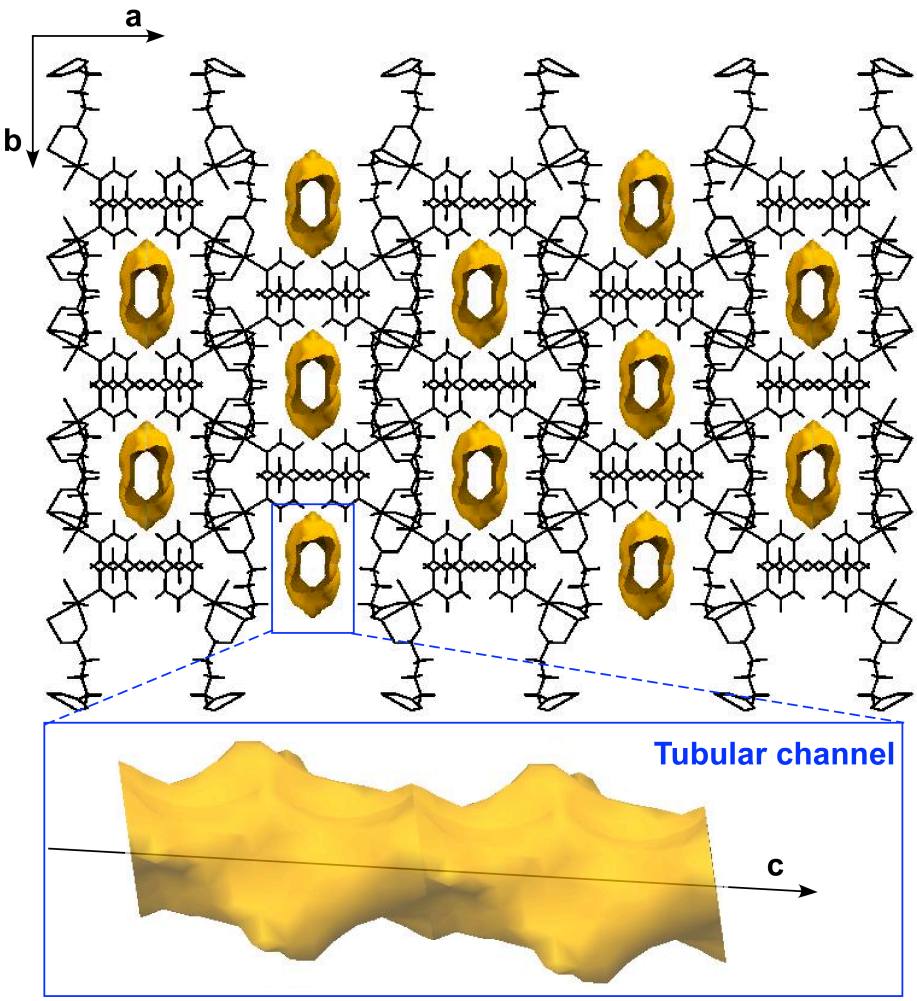

Figure S8. Crystal packing of **GR-MOF-2** showing the 1D void system.

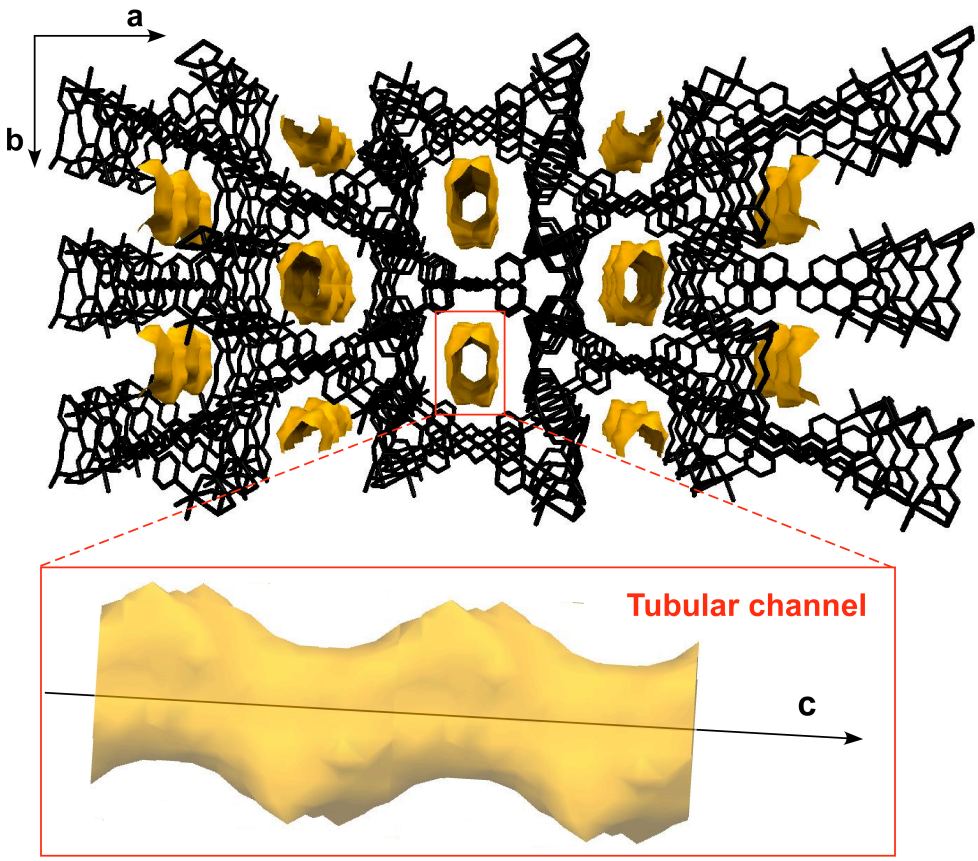

Figure S9. Crystal packing of **GR-MOF-3** showing the 1D void system.

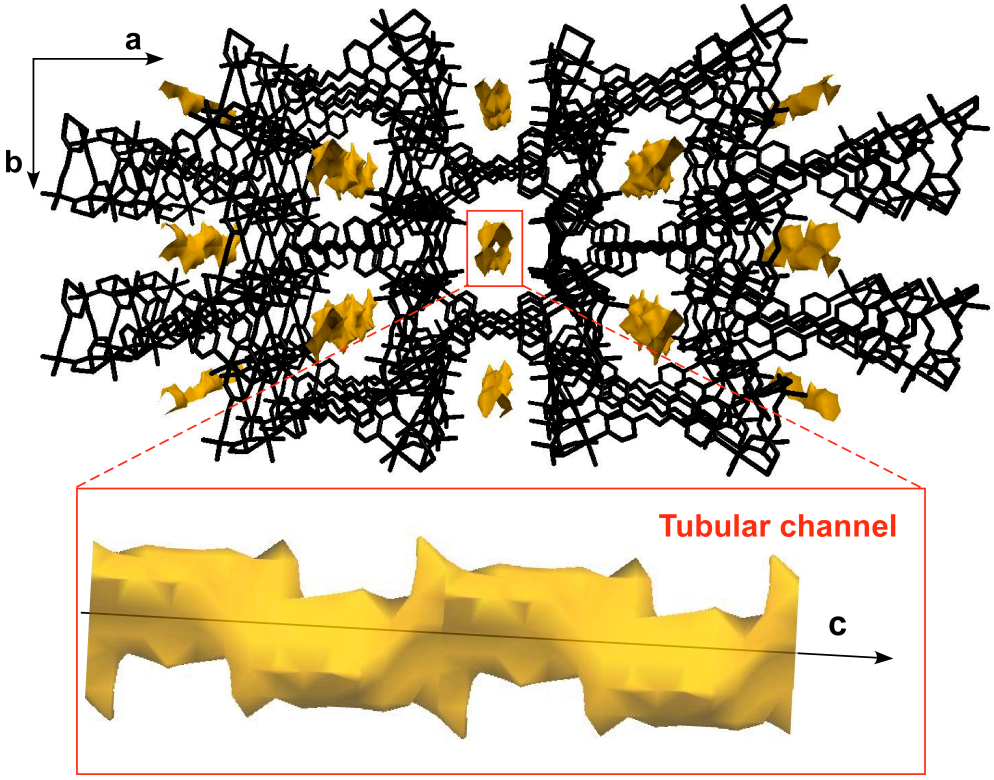

Figure S10. Crystal packing of **GR-MOF-4** showing the 1D void system.

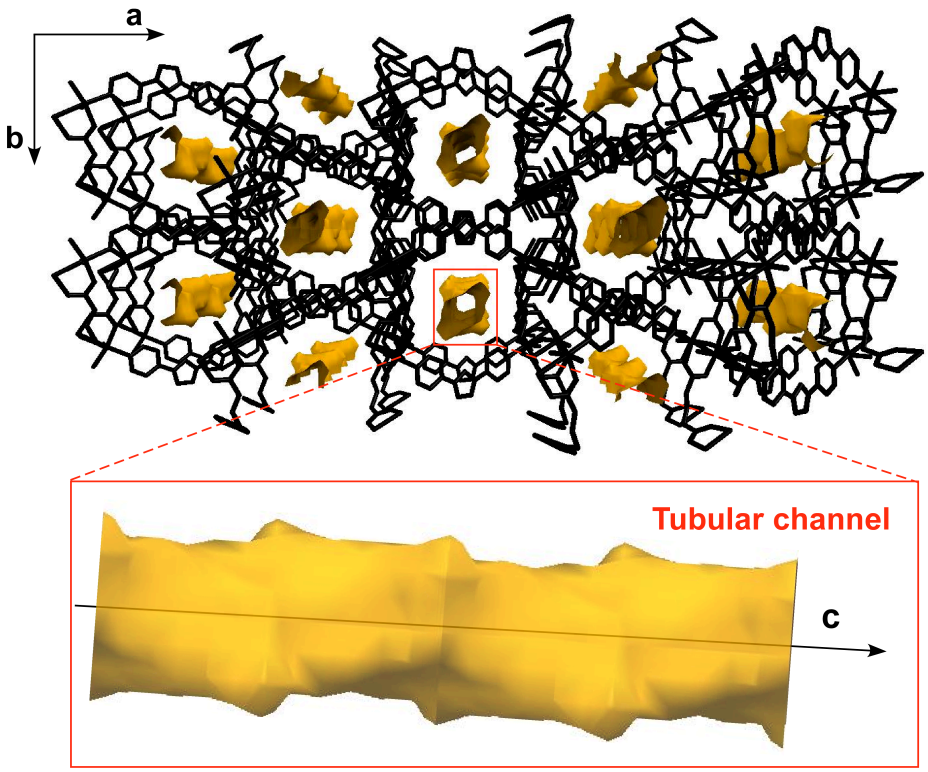

Figure S11. Crystal packing of **GR-MOF-5** showing the 1D void system.

S7. FT-IR spectroscopy.

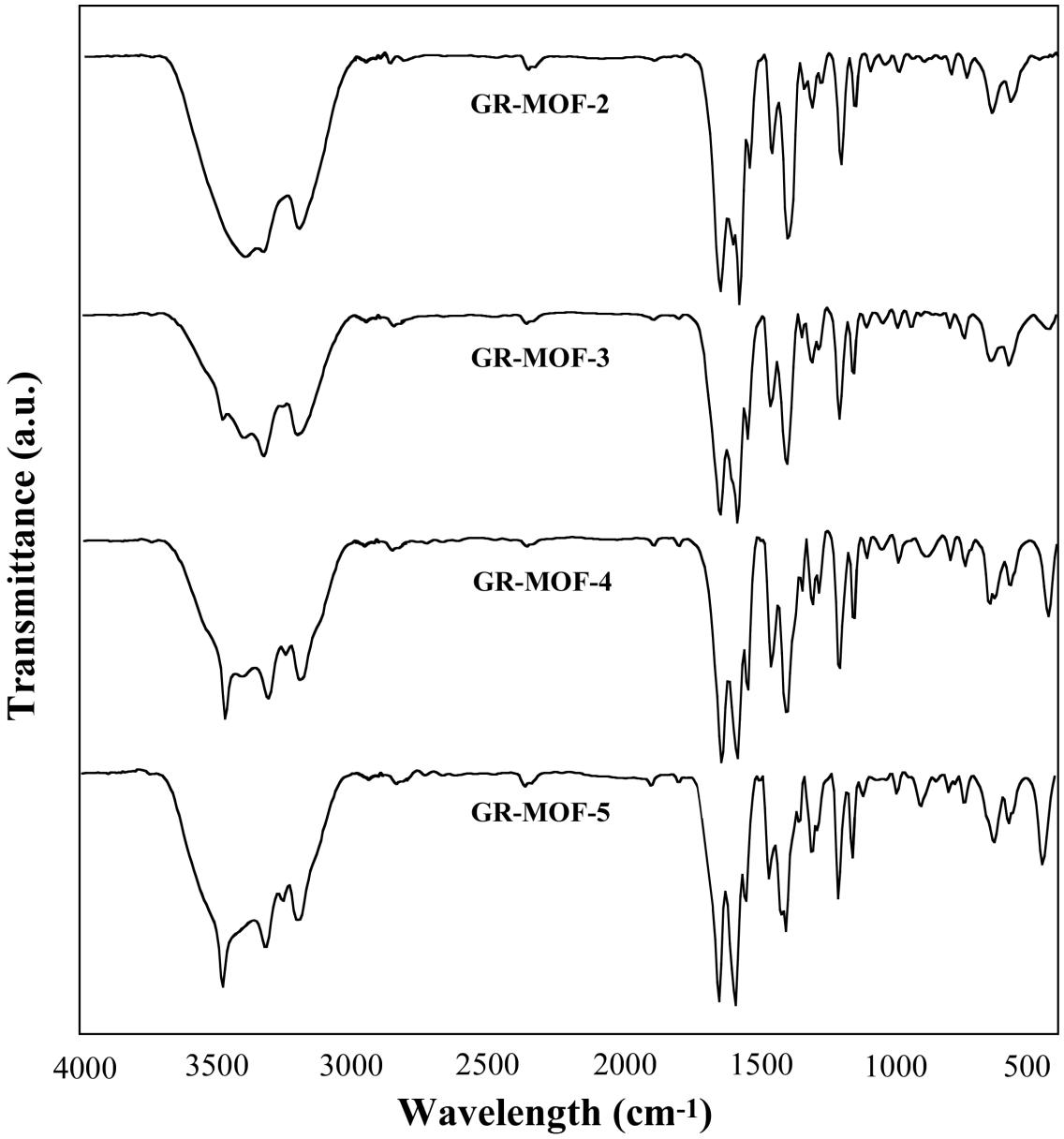

Figure S12. FTIR spectra of GR-MOFs.

S8. Adsorption measurements.

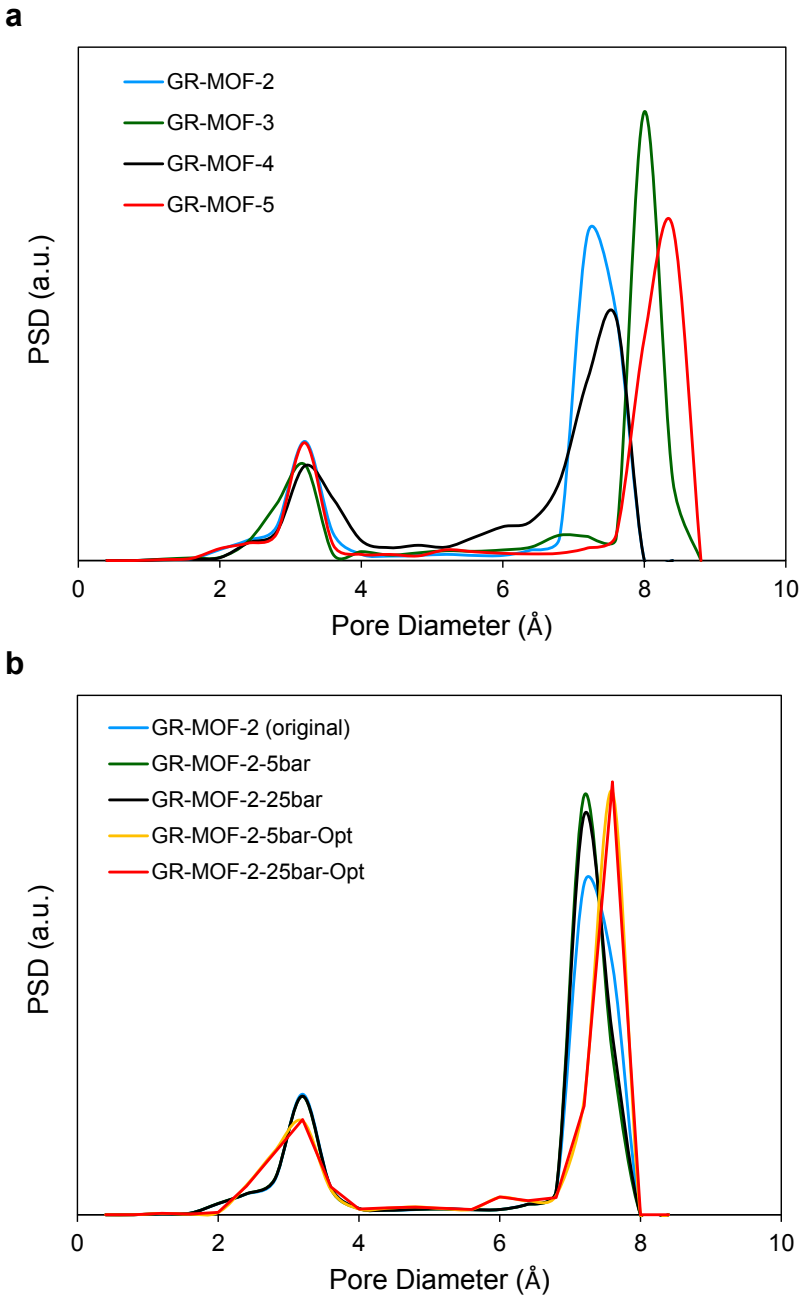

Figure S13. Pore size distribution of **a.** for all the GR-MOFs and **b.** Forcite-**GR-MOF-2** modified structures.

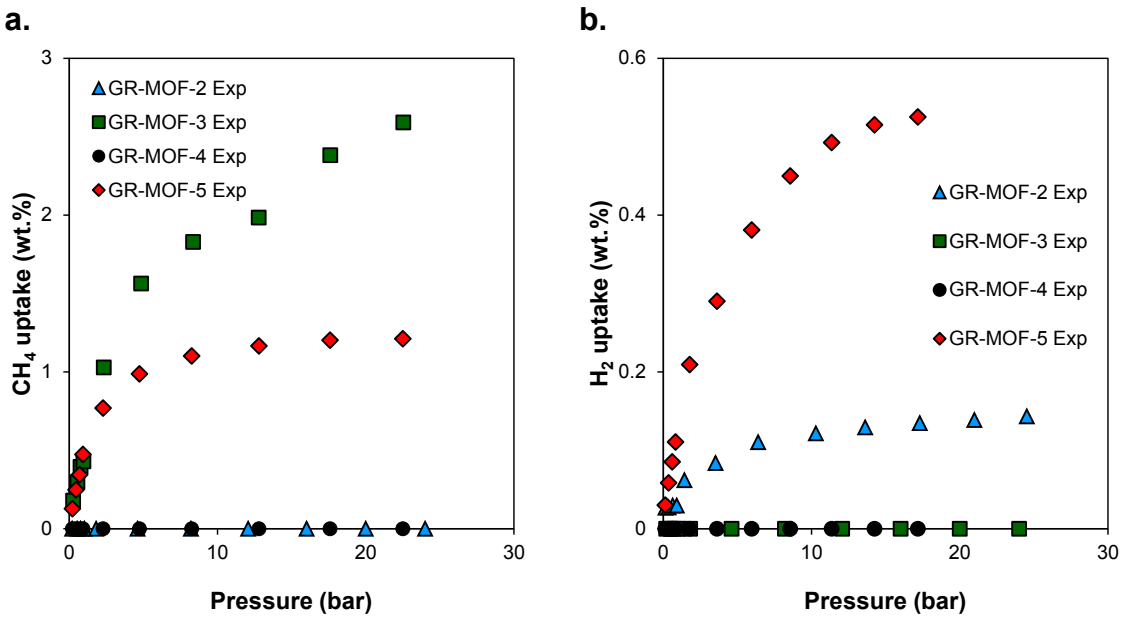

Figure S14. Experimental adsorption isotherms of **a.** CH_4 at 273 K and **b.** H_2 at 77 K for all the GR-MOFs.

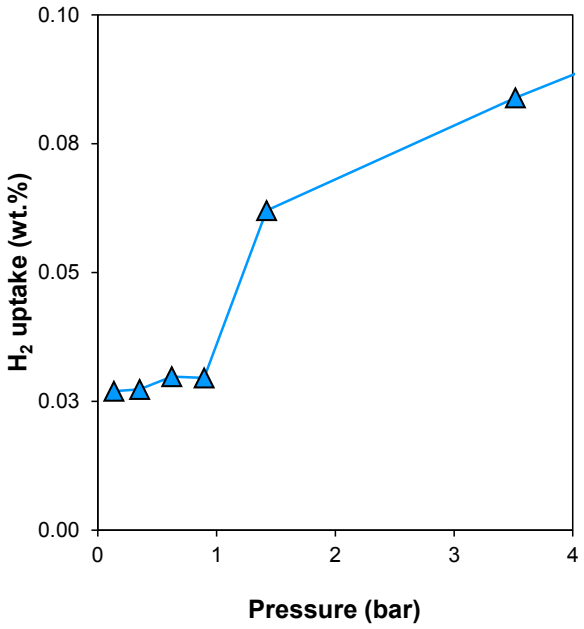

Figure S15. Details of the experimental adsorption isotherm of H_2 at 77 K on **GR-MOF-2**.

GR-MOFs characterize for flexible structures according to "accordion" shaped arrangement shown in Figure S12. This flexibility is particularly noticed when subjecting the samples to high pressures during adsorption experiments. Therefore, this behavior was studied by means of X-ray diffraction on **GR-MOF-4**, in such a way that the evolution of the unit cell parameters could be observed under variable pressures. As observed, raising the pressure from 0 to 5 bar brings a sharp drop of *a* and *β* lattice parameters, whereas *b* and *c* parameters are accordingly increased, all of which is translated into the compression of the structure (lattice volume is decreased). Hereafter, an inflection point is observed at ca. 8 bar, above which *a* and *β* parameters slightly recover the initial value whereas *b* and *c* parameters are levelled off. As a consequence, the increase in the pressure brings an expansion of the unit cell. Taking into account that microchannels are parallel to the crystallographic *c* axis, this evolution involves that microchannels are compressed at low pressures (from 0 to 5 bar) and recover their initial shape as they get filled with absorbates, in such a way that almost stabilised at P < 10 bar.

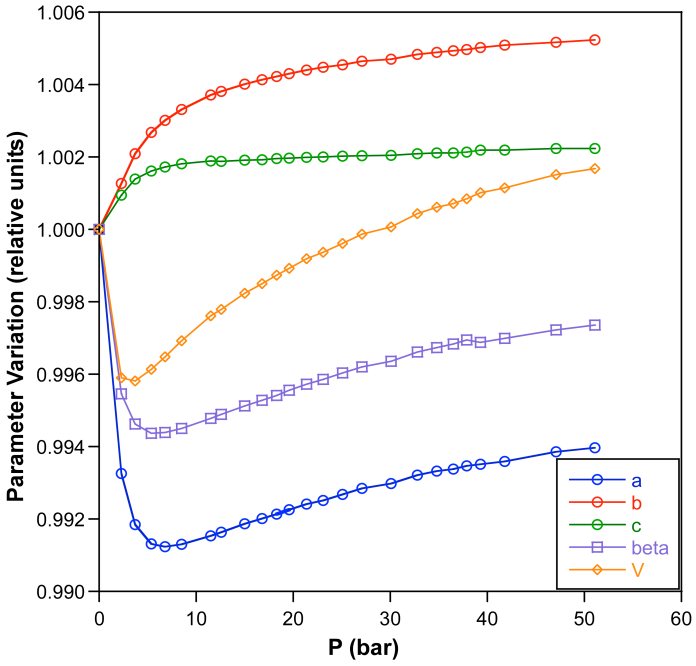

Figure S16. Pressure-dependent evolution of the unit cell parameters of **GR-MOF-2** during the adsorption of CO_2 at 273 K.

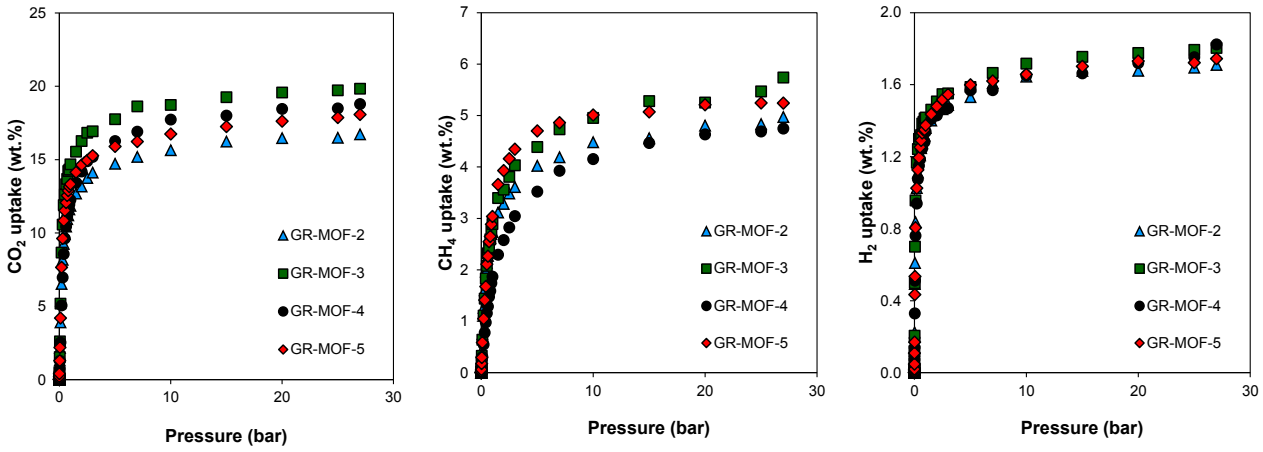

Figure S17. GCMC simulated adsorption isotherms of CO_2 at 273 K (*left*), CH_4 at 273 K (*center*) and H_2 at 77 K (*right*) for all the GR-MOFs.

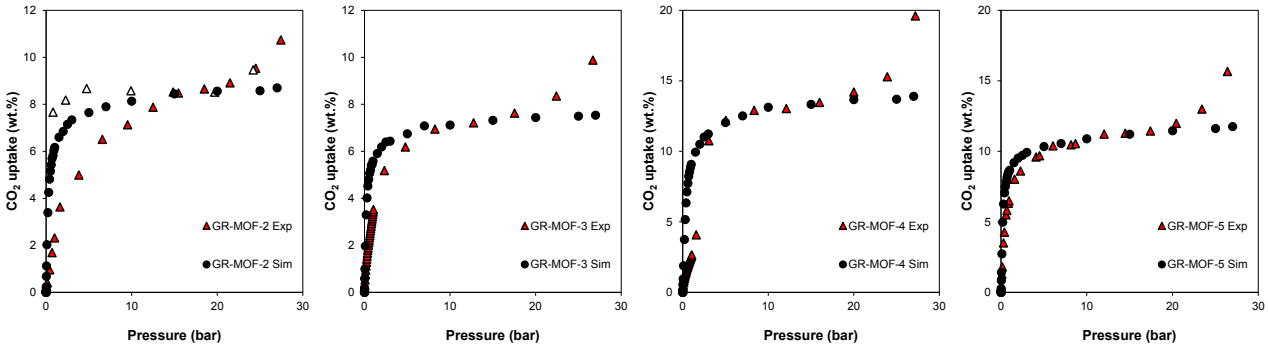

Figure S18. Comparison of CO_2 adsorption isotherms at 273 K for all the GR-MOFs: experimental adsorption, red triangles, and desorption, empty triangles, as well as simulated, black circles.